Supplementary Material for

Robust Spin-Valley Coupling in Hexagonal Monolayers of Tl-Based Monochalcogenides

Kang Sheng and Zhi-Yong Wang*

School of Physical Science and Technology,

Southwest University, Chongqing 400715, China and

Chongqing Key Laboratory of Micro-Nano Structure Optoelectronics, Chongqing 400715, China

* Corresponding author: zywang@swu.edu.cn

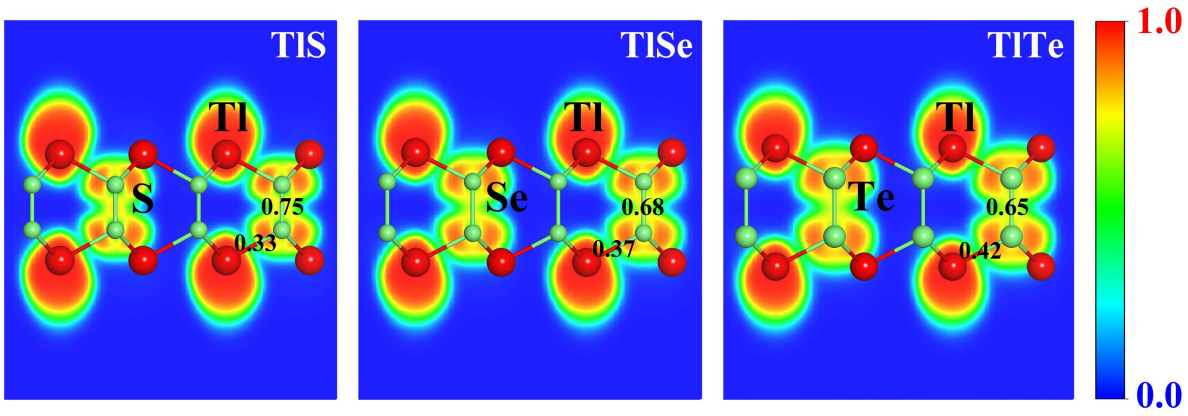

Fig. S1: Maps of electron localization function (ELF) for monolayer TlX (X = S, Se, Te) over the (110) plane, which is renormalized to values between 0.0 for vanishing charge and 1.0 for completely localized charge. The ELF is defined as ELF = $\frac{1}{1+\{K(r)/K_{\mathrm{u}}[\rho(r)]\}^2}$ [1], where K denotes the curvature of electronic pair density for electrons with the identical spin, $\rho(r)$ represents the electron density at position r, and $K_{\mathrm{u}}[\rho(r)]$ is the K value in a uniform electron gas with density $\rho(r)$. Values greater than 0.5 correspond to covalent bonds or core electrons, values less than 0.5 refer to ionic bonds, and value equal to 0.5 implies a uniform electron gas with metallic bond features. It is clear that the shared-electron interactions can be found between two vertically arranged chalcogen atoms, and thus the X-X bonds show the weak covalent bonding nature. On the other hand, the neighboring Tl and X atoms display an ionic bonding character.

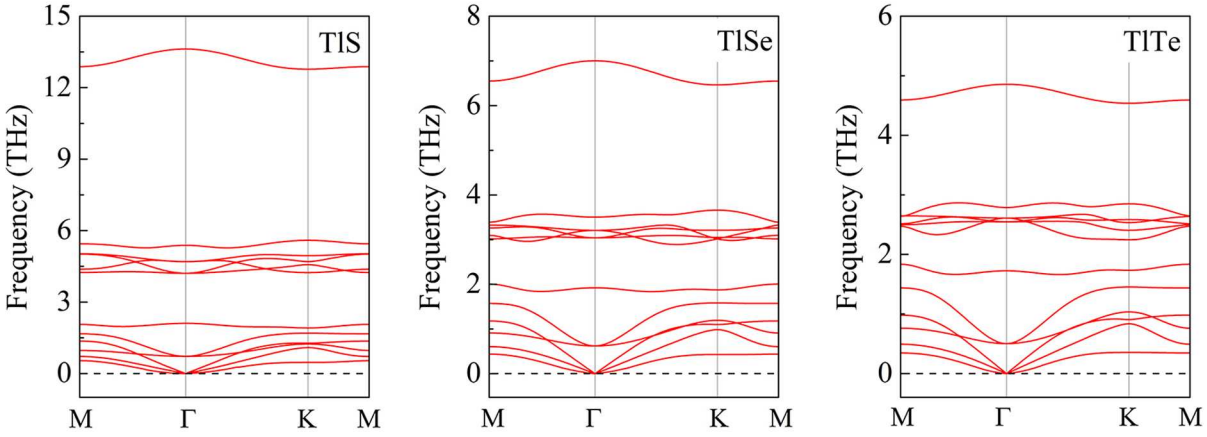

Fig. S2: Phonon dispersions for monolayer TlX (X = S, Se, Te) derived from density functional perturbation theory [2] on a $3 \times 3 \times 1$ supercell as implemented in the PHONOPY package [3]. Note that the phonon spectrum in monolayer TlS exhibits minuscule imaginary frequencies in the vicinity of the Γ point, which arises from the numerical uncertainties in first-principles calculations rather than the real instability of this material. A similar artifact has been observed as well in other 2D materials such as the well-known graphene system [4]. These spurious imaginary modes can be eliminated by adopting larger supercells and denser **k**-point grids at the expense of harsher computational costs [5].

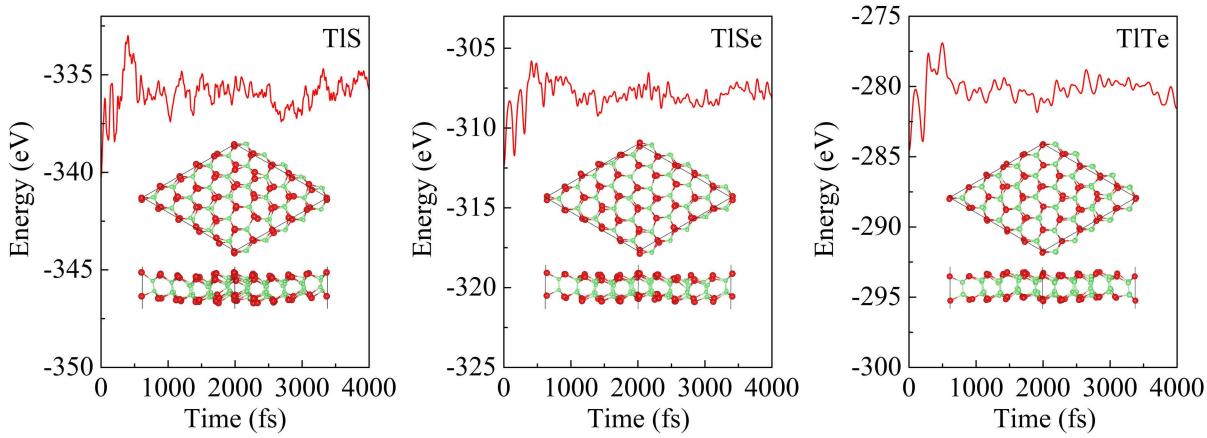

Fig. S3: Evolution of potential energies for monolayer TlX (X = S, Se, Te) from 4.0 ps *ab initio* molecular dynamics simulations with a time step of 1.0 fs on a $5 \times 5 \times 1$ supercell at 300 K with a Nosé-Hoove thermostat [6]. The insets display the corresponding snapshots at the end of each simulation, all of which can quickly recover their initial equilibrium configurations after performing geometry optimization.

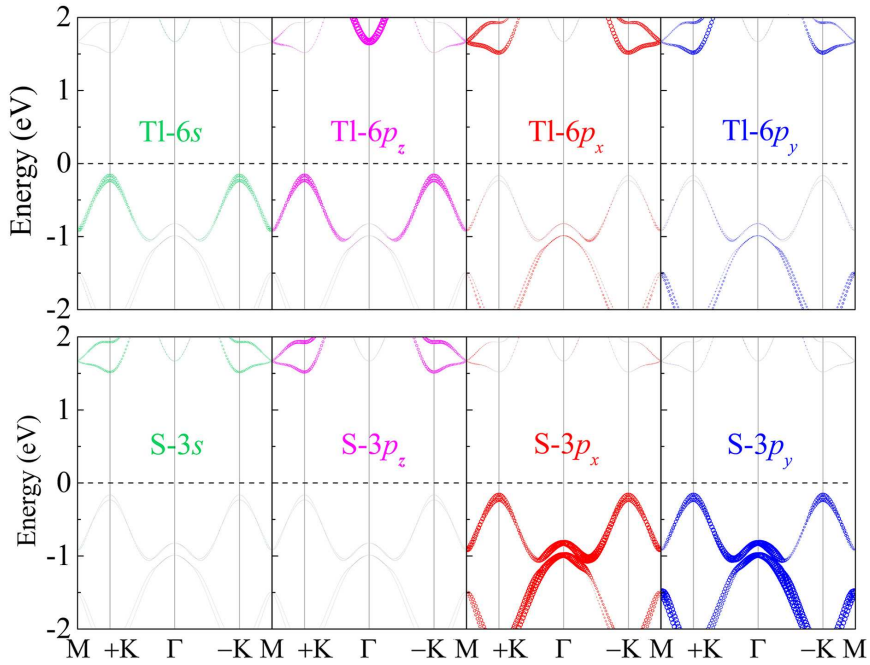

Fig. S4: Orbital-resolved band structures of monolayer TlS at the HSE06 + SOC level. The size of symbols is proportional to the corresponding orbital weight and the Fermi level is set to zero.

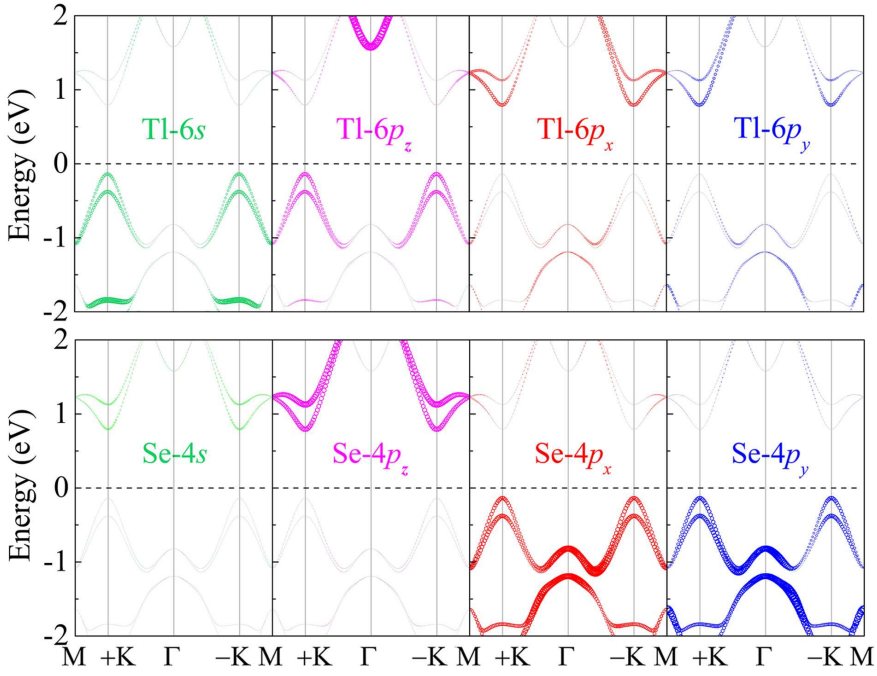

Fig. S5: Orbital-resolved band structures of monolayer TlSe at the HSE06 + SOC level. The size of symbols is proportional to the corresponding orbital weight and the Fermi level is set to zero.

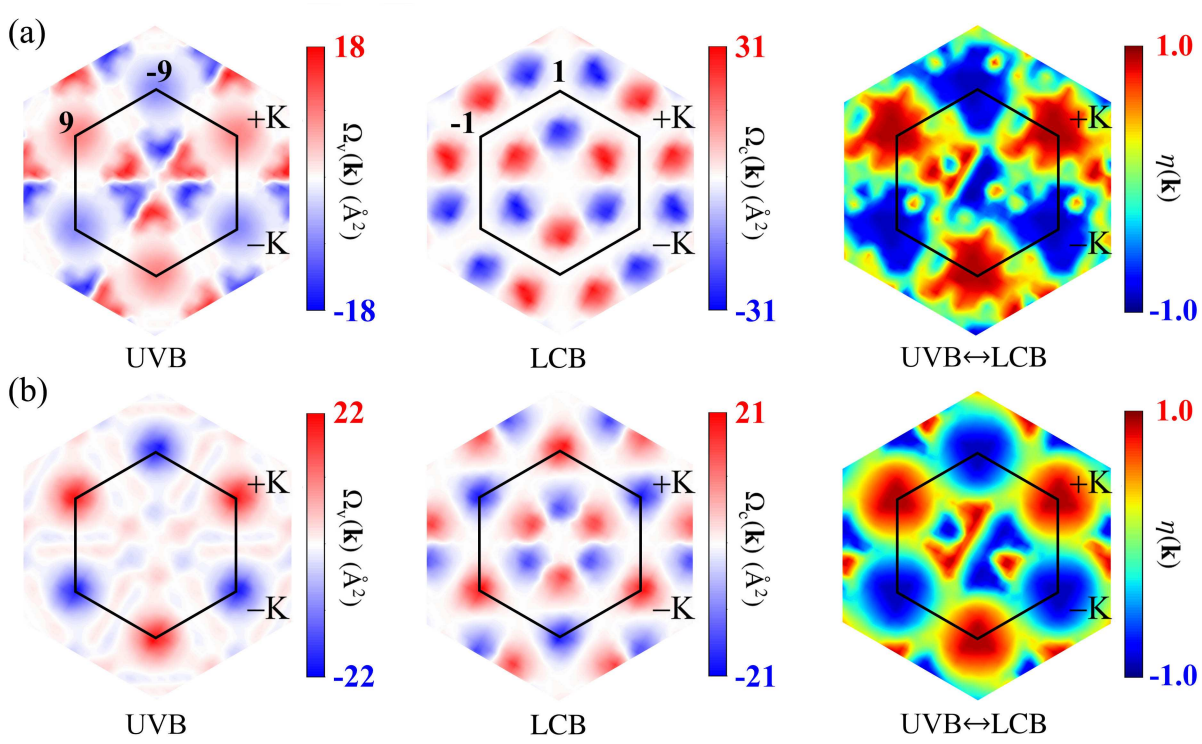

Fig. S6: (a) Berry curvatures for UVB and LCB over the 2D Brillouin zone as well as momentum-resolved normalized circular polarization for optical transition from UVB to LCB in monolayer TlS. Note that $\Omega_v(+K) = -\Omega_v(-K) = 9$ Å^2 and $\Omega_c(+K) = -\Omega_c(-K) = -1$ Å^2. (b) Same as those in (a) but for monolayer TlSe where $\Omega_v(+K) = -\Omega_v(-K) = 22$ Å^2 and $\Omega_c(+K) = -\Omega_c(-K) = -21$ Å^2. It is clear that the Berry curvature at the ±K valleys is larger in monolayer TlSe than in TlS on account of strong SOC interaction arising from heavier chalcogen atoms. In either system, the circular dichroism is perfectly valley-selective owing to the protection of C_3 rotational symmetry, implying that the frequency-specific left-handed (σ^+) and right-hand (σ^-) circularly polarized light can exclusively excite the +K and −K valley, respectively. As a consequence, the population imbalance of charge carriers in the two valleys can be generated via selective optical pumping, which is essential to achieve the charge, spin, and valley Hall effects simultaneously.

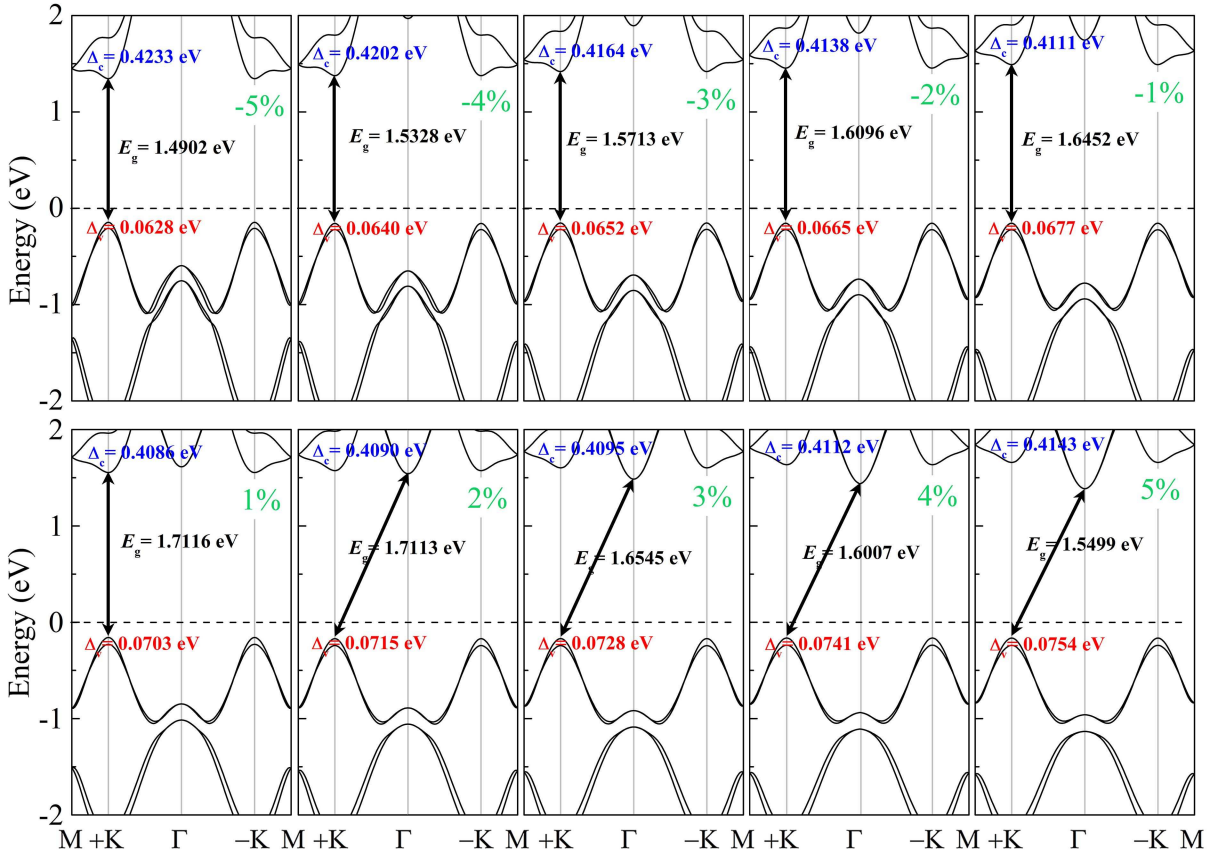

Fig. S7: Spin-split band structures of monolayer TlS at the HSE06 + SOC level under different biaxial strains ranging from −5% to +5% with the − and + symbols referring respectively to the compressive and tensile strains. Also shown are the bandgap and valley spin splittings in the conduction and valence bands.

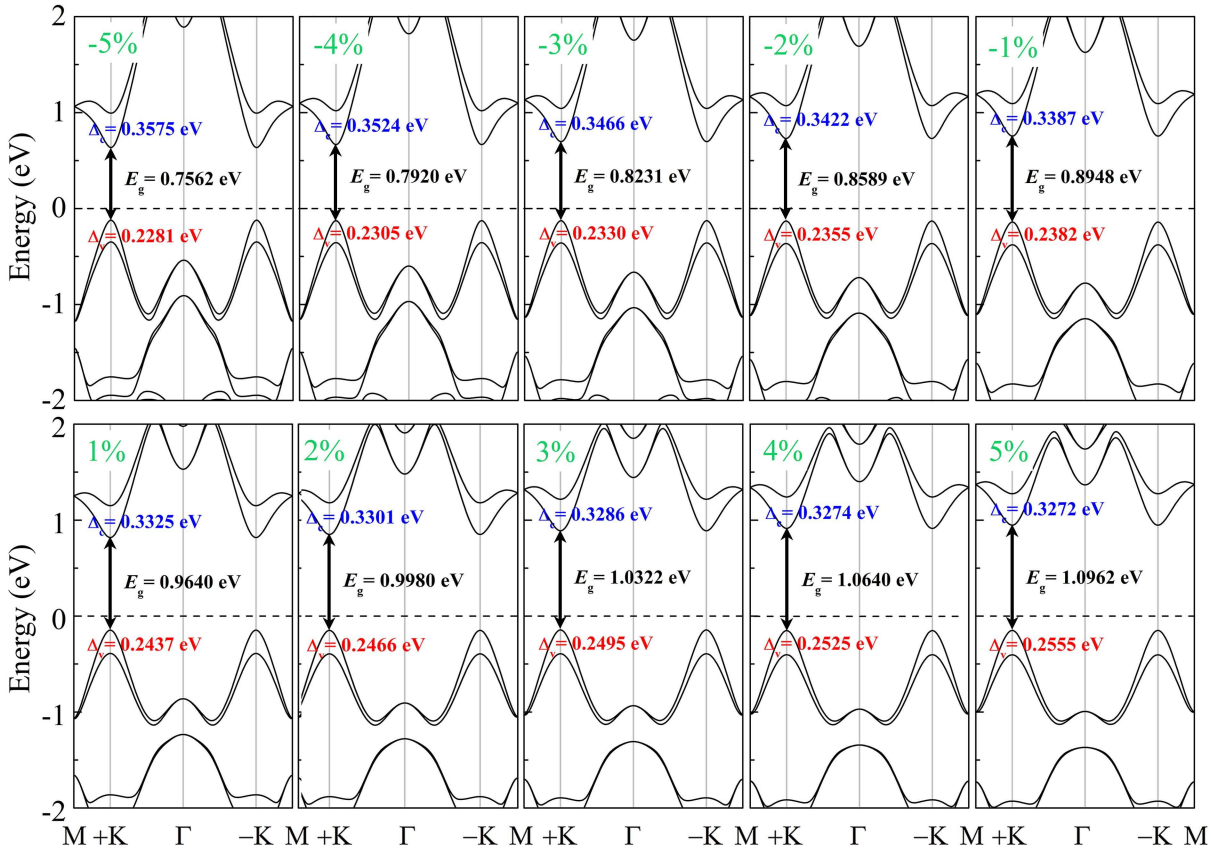

Fig. S8: Spin-split band structures of monolayer TlSe at the HSE06 + SOC level under different biaxial strains ranging from −5% to +5% with the − and + symbols referring respectively to the compressive and tensile strains. Also shown are the bandgap and valley spin splittings in the conduction and valence bands.

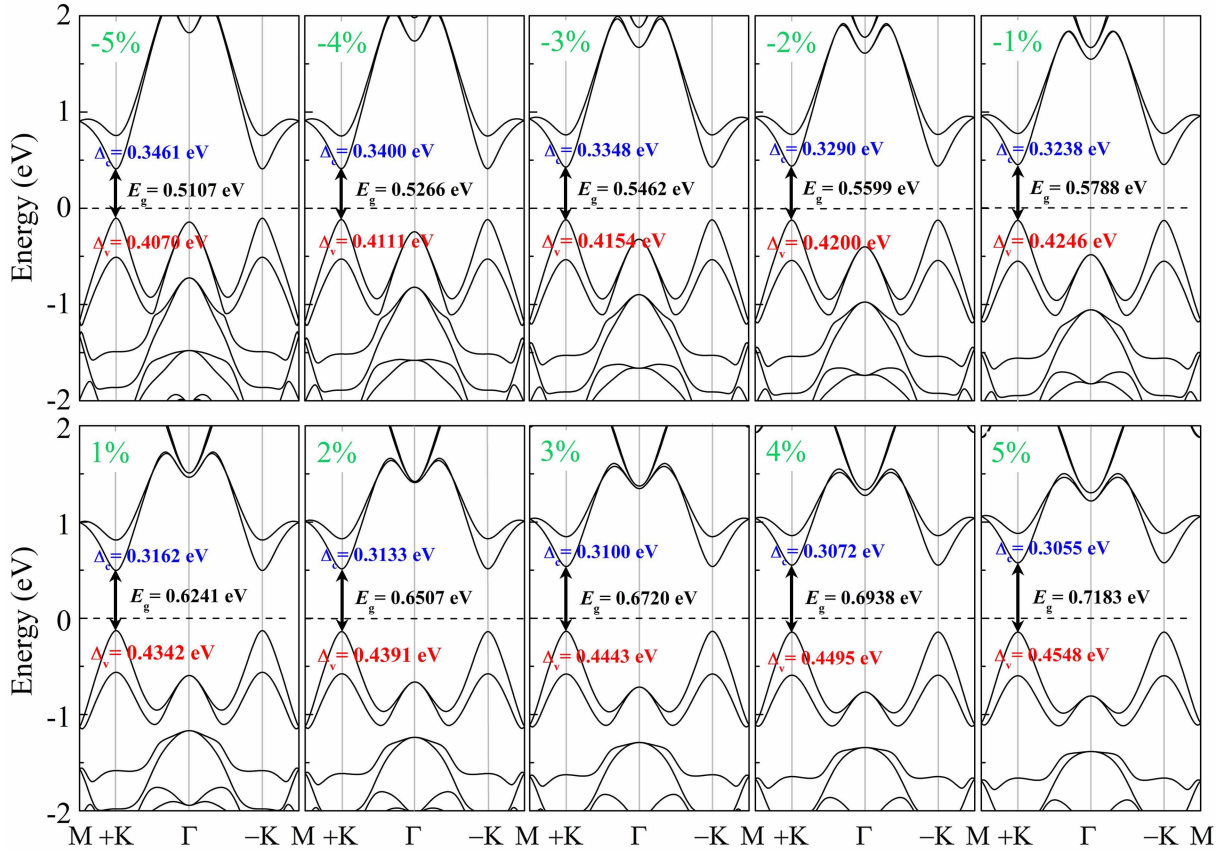

Fig. S9: Spin-split band structures of monolayer TlTe at the HSE06 + SOC level under different biaxial strains ranging from −5% to +5% with the − and + symbols referring respectively to the compressive and tensile strains. Also shown are the bandgap and valley spin splittings in the conduction and valence bands.

[1] A. Savin, O. Jepsen, J. Flad, O. K. Anderson, H. Preuss, and H. G. von Schnering, Electron Localization in Solid-State Structures of the Elements: the Diamond Structure, Angew. Chem. Int. Ed. **31**, 187 (1992).

[2] S. Baroni, S. de Gironcoli, A. Dal Corso, and P. Giannozzi, Phonons and related crystal properties from density-functional perturbation theory, Rev. Mod. Phys. **73**, 515 (2001).

[3] A. Togo and I. Tanaka, First principles phonon calculations in materials science, Scr. Mater. **108**, 1 (2015).

[4] Z. W. Tan, J.-S. Wang, and C. K. Gan, First-principles study of heat transport properties of graphene nanoribbons, Nano Lett. **11**, 214 (2011).

[5] H. Chen, P. Tang, and J. Li, Two-dimensional intrinsic ferromagnetic monolayer transition metal oxy-hydroxide, Phys. Rev. B **103**, 195402 (2021).

[6] G. J. Martyna, M. L. Klein, and M. Tuckerman, Nosé-Hoover chains: The canonical ensemble via continuous dynamics, J. Chem. Phys. **97**, 2635 (1992).